ASTM INTERNATIONAL

Journal of Testing and Evaluation

Rosario Fedele,[1] Filippo Giammaria Praticò,[2] and Gianfranco Pellicano[2]

DOI: 10.1520/JTE20190209

The Prediction of Road Cracks through Acoustic Signature: Extended Finite Element Modeling and Experiments

Journal of Testing and Evaluation

doi:10.1520/JTE20190209 available online at www.astm.org

Rosario Fedele,[1] Filippo Giammaria Praticò,[2] and Gianfranco Pellicano[2]

The Prediction of Road Cracks through Acoustic Signature: Extended Finite Element Modeling and Experiments

Reference

R. Fedele, F. G. Praticò, and G. Pellicano, "The Prediction of Road Cracks through Acoustic Signature: Extended Finite Element Modeling and Experiments," *Journal of Testing and Evaluation* https://doi.org/10.1520/JTE20190209

ABSTRACT

Traffic produces vibrations and noise that affect the livability and structural integrity of the built environment. Despite the fact that many studies focused on traffic-induced vibrations and noise, there is a lack of studies linking the vibrations propagating into the road pavement and the related acoustic response (or acoustic signature) as a means to assess the structural health status. Indeed, monitoring this response can lead to an estimation of the road layer structural condition and an identification of cracks that occurred because of the traffic. Consequently, the objectives of this study are to (i) model the involved phenomena through a Finite Element Method (FEM) analysis; (ii) compare data and simulations; and (iii) set up an Extended Finite Element Model (EXFEM) that is able to forecast the change of the road acoustic signature over time because of the presence of occurred cracks. Loads and sound-related phenomena (generation, transmission, interaction with cracks) were simulated through an EXFEM software. In addition, in order to estimate the effectiveness of the study, the aforementioned simulations were compared with real data gathered from a Dense Graded Friction Course road pavement in different and controlled structural conditions through a specially designed, microphone-based electronic system. Even if further studies are needed to better fix the measurement chain and better carry out the FEM analyses, preliminary results show that the EXFEM model is able to reproduce, with good approximation, the measured signals and that this model can be used to forecast the effects of different types of cracks on the propagation of vibration into road pavements.

Keywords

pavement, noise, vibration, cracks, Extended Finite Element Model, acoustic signature, structural health monitoring

Manuscript received March 13, 2019; accepted for publication July 29, 2019; published online September 19, 2019.

[1] DIIES Department, University Mediterranea of Reggio Calabria, Via Graziella - Feo di Vito, Reggio Calabria 89100, Italy (Corresponding author), e-mail: rosario.fedele@unirc.it, https://orcid.org/0000-0002-7312-6726

[2] DIIES Department, University Mediterranea of Reggio Calabria, Via Graziella - Feo di Vito, Reggio Calabria 89100, Italy, https://orcid.org/0000-0003-3576-7976 (F.G.P.), https://orcid.org/0000-0003-2551-2603 (G.P.)

Introduction

Traffic produces vibrations and noise that have a negative impact on the livability, performance, and durability of the built environment that surrounds and includes the transportation infrastructures.

The aforementioned characteristics (effects) mainly depend on the same reason (cause), i.e., on road pavement conditions. Hence, the evaluation of the road pavement conditions and the prompt detection of damages (both surface and concealed) are crucial factors for the reduction of the negative impacts mentioned earlier.

As is well known, the level of comfort offered to the users by road pavements and their duration depends on the quality of the maintenance process. If a failure-based approach is used to schedule and carry out the maintenance interventions, complex and expensive works are needed.[1] On the other hand, if condition- or predictive-based approaches are used to manage maintenance and replacement of the roads, it is possible, at the same time, to (i) make the work of the authorities that are responsible for the management of the transportation infrastructures more sustainable (i.e., easier and cheaper) and (ii) offer to the users of these infrastructures high levels of comfort and reliability. Importantly, the literature[2] shows that if a road pavement is reconstructed when a potential failure (e.g., a hidden crack) is detected and the overall conditions of the road pavement are decreased to about 30 % with respect to the initial ones (as-built pavement), about $4 are needed per square yard (1 square yard = 0.84 m^2). In contrast, about $18 are needed if the reconstruction is carried out when function failures are present (easily detectable, such as a pothole) and the overall pavement conditions are about 20 % of the original ones. This means that[2] prompt detection of the symptoms leads to great advantages, which are related not only to money savings but also energy savings and carbon footprint reduction. In fact, money savings are primarily due to the energy saved because of the fact that maintenance interventions are reduced, and the reconstruction is postponed.

Currently, the failure-based approach is the most widespread and often uses local, expensive, and destructive tests (e.g., coring) or surface monitoring (e.g., using instrumented vehicles[3,4]) to detect damages, assess road pavement performance, and derive road conditions. In contrast, condition-based approaches need technologies that are able to constantly assess road conditions. Several solutions based on remote sensing methodologies[5] have been provided in the last decades. The main limits of the aforementioned solutions refer to the ability to detect only surface damages, while concealed damages are neglected. Usually, this aspect is underestimated, but it is important to underline that most of the surface damages are a consequence of the presence or propagation of one or more concealed distresses (a.k.a., bottom-up crack propagation). Hence, the detection and monitoring of hidden damages is a crucial factor of the road management process.

Trying to solve this problem, seismic and electromagnetic methods were proposed and improved (e.g., combining machine learning and Ground Penetrating Radar analysis[6] or using wavelet denoizing to improve Deflectometer-related measurements[7]). The main limits of these approaches refer to the need to interfere with traffic to carry out measurements, which are related only to the area of investigation. Recently, methods based on embedded sensors[8–10] were proposed, but several problems related to the installation, powering, and costs need to be solved before thinking to their implementations in real contexts.

In order to solve the aforementioned limits, predictive approaches based on a Finite Element Model can be taken into account. In particular, the application of solutions that are able to forecast the variation of the structural conditions of road pavements could be the key factor to improve the efficiency and sustainability of the current management processes. Relevant examples of Finite Element Method (FEM) applications related to the road infrastructures refer to the (i) derivation of road pavement dynamic response to different loads (using the software ABAQUS,[11–13] SAFEM,[14] and COMSOL Multiphysics[15]); (ii) estimation of the dynamic modulus of asphalt concrete pavements (using the software ABAQUS[16,17]); (iii) study of vehicle–pavement interaction for roads and bridges (using the software ABAQUS,[18] ANSYS,[19] MATLAB,[20] CAPA-3D,[21] and SURFER[22]); (iv) modeling of ground-borne vibrations due to the traffic (using the software ANSYS,[19] MATLAB,[20] COMSOL Multiphysics,[23] SURFER[22]); and (v) evaluation of road pavement deterioration (i.e., cracking or deformation[24]) and crack propagation (using the software ABAQUS[8,25–27] and SAFEM[28] and Artificial Neural Networks[29]).

Despite the fact that many studies focused on the effect of the traffic-induced effects on humans and structures that surround the road infrastructures, there is a lack of studies linking the vibrations propagating in the road pavement and the related vibro-acoustic response (or vibro-acoustic signature) as a means to assess the Structural Health Status (SHS). Consequently, the objectives of this study are to (i) model the involved phenomena through an FEM analysis, (ii) compare data and simulations, and (iii) set up an Extended Finite Element Model (EXFEM) that is able to forecast the change of the road acoustic signature over time because of the presence of occurred cracks. The remaining parts of this article are organized into the following main sections: "Problem Statement, Overall Framework, and Procedure Used," "Experimental Investigation," "FEM Modeling and Calibration," "Results of Calibration," and "Conclusions."

Problem Statement, Overall Framework, and Procedure Used

In this study, the overall conditions of the road pavement, which include the presence of surface or concealed damages, are indicated using the term "SHS." "Structural health" derives from Structural Health Monitoring, a strategy[30] that aims at identifying changes of the material and geometric properties (including variations of the boundary conditions) of different types of structures (e.g., buildings, roads, bridges[31,32]) that affect the current or future performance of these assets. This strategy has four main objectives with increasing levels of difficulty, i.e., (i) damage detection, (ii) damage localization, (iii) damage type identification, and (iv) damage level quantification. In this study, the term "SHS" refers to the temporal variations of the structural integrity of a road pavement (which varies from the as-built status to the failure), and the study, as mentioned at the end of the previous section, aims at carrying out damage detection.

An innovative Nondestructive Test (NDT)-based system (see fig. 1) has been set up in the pursuit of monitoring primarily concealed cracks of road pavements.[33–36] The system builds on vibration propagation in the pavement (Medium A = pavement) and consequent noise sound wave formation into the surrounding medium (Medium B = air), where Medium A is composed of pavement materials. The rationale behind this is the dependence of acoustic responses (ARs; acoustic signature) on the SHS of Medium A. The input to the system is given in 1 (e.g., wheel pass or load impact): it is a load that, for the given surface, is a function of time and corresponds to a given frequency spectrum.

A wave is generated in 1 (by the traffic) and propagates through the pavement, also toward the sensor located on the pavement. The wave has an ambivalent character, because at constant t (time), it is a harmonic function of the spatial variable x (distance), while at a constant x, it is a harmonic vibration, dependent on the time t at a given point.[37] The output (unknown), at a given distance x from the input, is another signal that varies over time and has another frequency spectrum (still unknown). It depends on input and pavement (Medium A aforementioned). Under given assumptions, the frequency response function links inputs and outputs in the frequency domain.[38,39] Because of the complexity of loads (vehicles), materials and structures (pavement), and involved phenomena, in order to better analyze results, an in-depth consideration of each factor involved is needed. To this end, the study presented in this article aims at modeling these phenomena through an FEM analysis and comparing data and simulations. An FEM-based approach is needed (i) because of its potential to predict

FIG. 1

Problem statement: schematic representation.

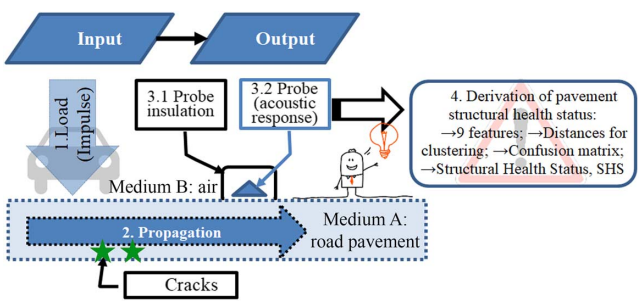

the response of the system; (ii) because FEM models offer the possibility to simulate several types of conditions (e.g., damage type, temperature change, thickness of the pavement layers, loads, etc.); (iii) because of the difficulty in using closed-form equations to solve these problems; and (iv) because of the need to double check if experimental responses are well-grounded in logic and the physics behind them is well understood.

In terms of overall framework of the research program, at the end of the setup process, the FEM model shall be able to simulate the variation of the road pavement vibro-ARs to traffic-induced sound and vibrations because of the presence of an increasing number of cracks into the pavement. This information is used to assess the current structural condition of the road pavement to forecast its remaining lifetime and design proper maintenance intervention to increase the performance (i.e., road without potholes) and safety level (e.g., reduce the number of accidents caused by a deteriorated or damaged road pavement) of the infrastructure. In more detail, the entire research project aims to:

(i) measure (experimental investigation) the ARs of a road pavement to mechanical loads produced by vehicles;
(ii) characterize the ARs previously cited by means of meaningful features (i.e., able to link the SHS of a pavement to its ARs) extracted in different domains of analysis;
(iii) set up an FEM model able to replicate (in terms of signals in the time domain and features) the ARs measured during the aforementioned experimental investigation;
(iv) evaluate the reliability and level of detail of the FEM model setup by comparing the features extracted from the measured ARs with those extracted from the ARs simulated using the FEM model; and
(v) use the FEM model to forecast the variation of the AR of a road pavement because of a variation of its SHS, which in turn is due to the presence of several types of cracks simulated using the FEM model.

Consequently, a specific procedure, shown in **figure 2**, was defined for this study. This procedure consists of the following steps:

Step 1: Measurement of the ARs of the pavement under test through a specially designed experimental investigation. In more detail, the road pavement was loaded using a Lightweight Deflectometer (LWD). A set of ARs of the uncracked road pavement (i.e., SHS 0, in the following SHS0) corresponding to a set of LWD loads is recorded using a microphone-based electronic system. The temperatures of the pavement surface and the air were measured during the experiments. Then, the SHS of the road pavement was changed by drilling several lines of holes in the middle between the receiver module and sources (to simulate the area of the carriageway where the traffic load is usually concentrated, i.e., the wheel paths). A set of ARs were recorded after the drilling of each line of holes.

FIG. 2

Framework of the study. Symbols: ARs (t) = ARs of the road pavement to a mechanical load in the time (t) domain; PSD (f) = Periodograms in the frequency domain (PSD versus frequency, f); S (t, f) = Scalograms using the Continuous Wavelet Transform in the time-frequency (t, f) domain; cf. § 3: compare with the "Experimental Investigation" section of this article.

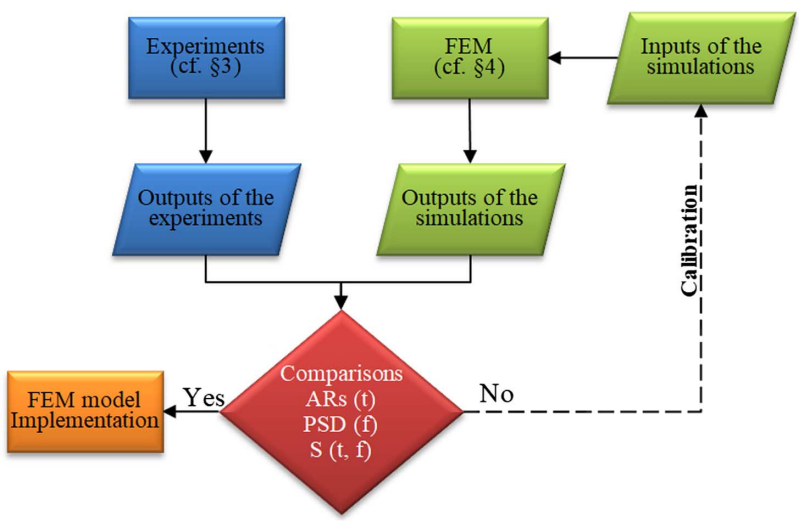

Step 2: Extraction of a set of features (i.e., time lags and peak ratios of seven peaks, which are shown in section "FEM Modeling and Calibration") from the ARs collected during Step 1.

Step 3: Setup of an FEM model by changing several input parameters to obtain simulated signals that replicate the measured ones.

Step 4: Comparison of the measured and simulated ARs in different domains of analysis, i.e., the ARs in the time domain (called ARs [t] in fig. 2), Periodograms (called *PSD* [f], in fig. 2) in the frequency domain, and Scalograms (called S [t, f] in the time-frequency domain) obtained using the Continuous Wavelet Transform (preliminary results showed that this tool allows obtaining graphical results, i.e., the Scalograms, which are able to show the variation of the ARs in the time-frequency domain better than other tools, such as the Discrete Wavelet Transform and the Short Time Fourier Transform).

Step 5: Use of the FEM model to forecast the variation of the ARs of the road pavement due to the presence of several types of simulated damages (surface and concealed) in order to (i) recognize the occurrence, propagation, or both of the damages mentioned earlier and (ii) forecast the status that represents the end of the lifetime of the road pavement.

Experimental Investigation

The experimental investigation presented in this study was carried out using a specially designed microphone-based electronic system (see fig. 3) and according to the results obtained in previous studies carried out by the same authors of this article.[34–36]

In general, the method applied in this study aims at detecting the generation of hidden cracks in road pavements, which are usually generated under the wheel paths, and monitoring their bottom-up propagation (toward the wearing course) due to the vehicular traffic. It is expected that presence, position, and size of cracks affects the road pavement acoustic behavior acting on specific frequency components, i.e., those related to waves whose wavelength depend on cracks' size. Hence, the generation of constructive and destructive interferences leads to the amplification or reduction of some spectral components of the response signals. As is well known, excessive loads (heavy vehicles), unexpected phenomena (e.g., earthquakes), fatigue phenomena (repeated loads, temperature excursions), or all are responsible for the generation and propagation of bottom-up cracks.

In order to control, as much as possible, the experimental conditions, the following strategy was adopted: (i) use a known source, i.e., an LWD, to load the pavement; (ii) use holes in order to control the road damaging, and (iii) study the variation of the road ARs to a known load because of the variation of the number of holes. It is important to underline that, because of the cracks' size, the position, and the propagation path, the drilled holes aimed at simulating bottom-up cracks at a highly advanced stage.

The study presented in this article is the first part of a wider research project (described in the "Problem Statement, Overall Framework, and Procedure Used" section). At the moment, the study does not aim at

FIG. 3

Measurement chain.

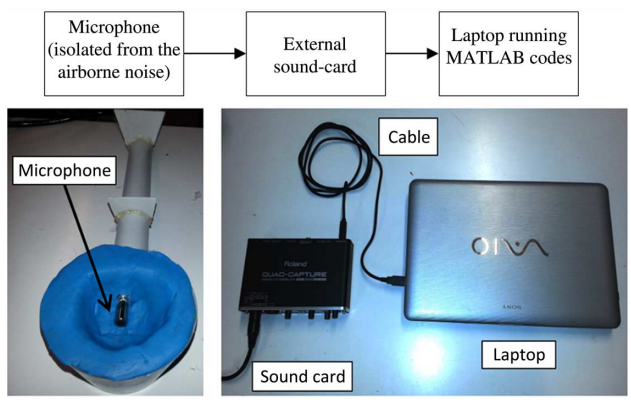

identifying the type of cracks or type of crack propagation, but it is focused on the setup of an FEM model that is able to simulate both the induced cracks and ARs of a road pavement (cracked and uncracked) to the LWD load (instead of the traffic). Subsequently, after a proper calibration, the aforementioned model can be used to forecast and control the variation of the ARs of other sections of the same pavement, simulating (i) the loads generated by whatever vehicles and (ii) the presence and propagation of whatever type of damage (e.g., hidden cracks).

This investigation was carried out in order to obtain the road pavement vibro-ARs to impulse loads (produced by an LWD), as a function of its SHS. In more detail, six SHSs were considered: SHS0 (i.e., no holes, or uncracked road), SHS1 (i.e., 1 line of holes), SHS2 (i.e., 2 lines of holes), SHS3 (i.e., 3 lines of holes), SHS4 (i.e., 4 lines of holes), and SHS5 (i.e., 5 lines of holes). The road pavement used in this study is a Dense Graded Friction Course (DGFC) air void content of 7 %, density of 2.32 t/m^3, with an age of five years, located in Southern Italy, with an average annual daily traffic of 2,000 vehicles per day.

The experimental investigation was carried out using a properly designed measurement chain (described in the following).

MEASUREMENT CHAIN

Figures 3 and 4 show the measurement chain (different devices and cables) that was used to measure the vibro-AR of the road pavement used in this study. For load source, an LWD (model: PRIMA 100, Grontmij; cf. fig. 3*A*) was used that was able to produce an average impulse load of 100 kN (measured using the LWD's load cell).

In particular, the devices used to measure the AR of the DGFC pavement to the load generated by the LWD consisted of (see fig. 2*B*) (i) one omnidirectional pre-polarized microphone (model: Audix TM1, frequency response = 20–25 kHz +/−2 dB, sensitivity = 6 mV/Pa at 1 kHz, dynamic range = 112 dB); (ii) one external audio card (model: Roland QUAD-CAPTURE UA-55); and (iii) several connecting cables (model: Ultimo RCM-GBK-Prolite). The acoustic signals were recorded (sampling frequency = 192 kHz) using a laptop running a proper MATLAB code.

MEASURED SIGNALS IN THREE DOMAINS OF ANALYSIS

Figures 5–7 show the ARs of the differently cracked road pavement to the LWD loads, related Periodograms (Power Spectral Density, *PSD versus* Frequency), and Scalograms (Continuous Wavelet Coefficients [CWCs] in the time-frequency domain).

In more detail, Periodograms show the *PSD* as a function of the frequency. The PSD was derived using the following equation[38]:

$$PSD = 2 \cdot \frac{|FFT|^2}{N \cdot Fs}, \tag{1}$$

where FFT is the Fast Fourier Transform of the signal to be transformed; N is the length of the aforementioned signal; Fs is the sampling frequency used to record the signals (Hz); and PSD is the power of the signal per unit of frequency, i.e., Watt per Hertz or dBW/Hz (if the decibel scale is used to represent the PSD).

FIG. 4

Experimental setup: microphone (R) placed on the (*A*) uncracked and (*B*) cracked road pavement (five lines of holes were indicated using Roman numerals from I to V) loaded with the LWD (S).

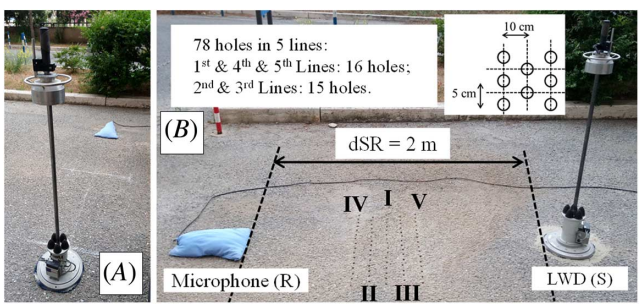

FIG. 5 ARs of the road pavement to the LWD loads: structural health statuses 0 to 5 (*A*–*F*) and their comparison (*G*).

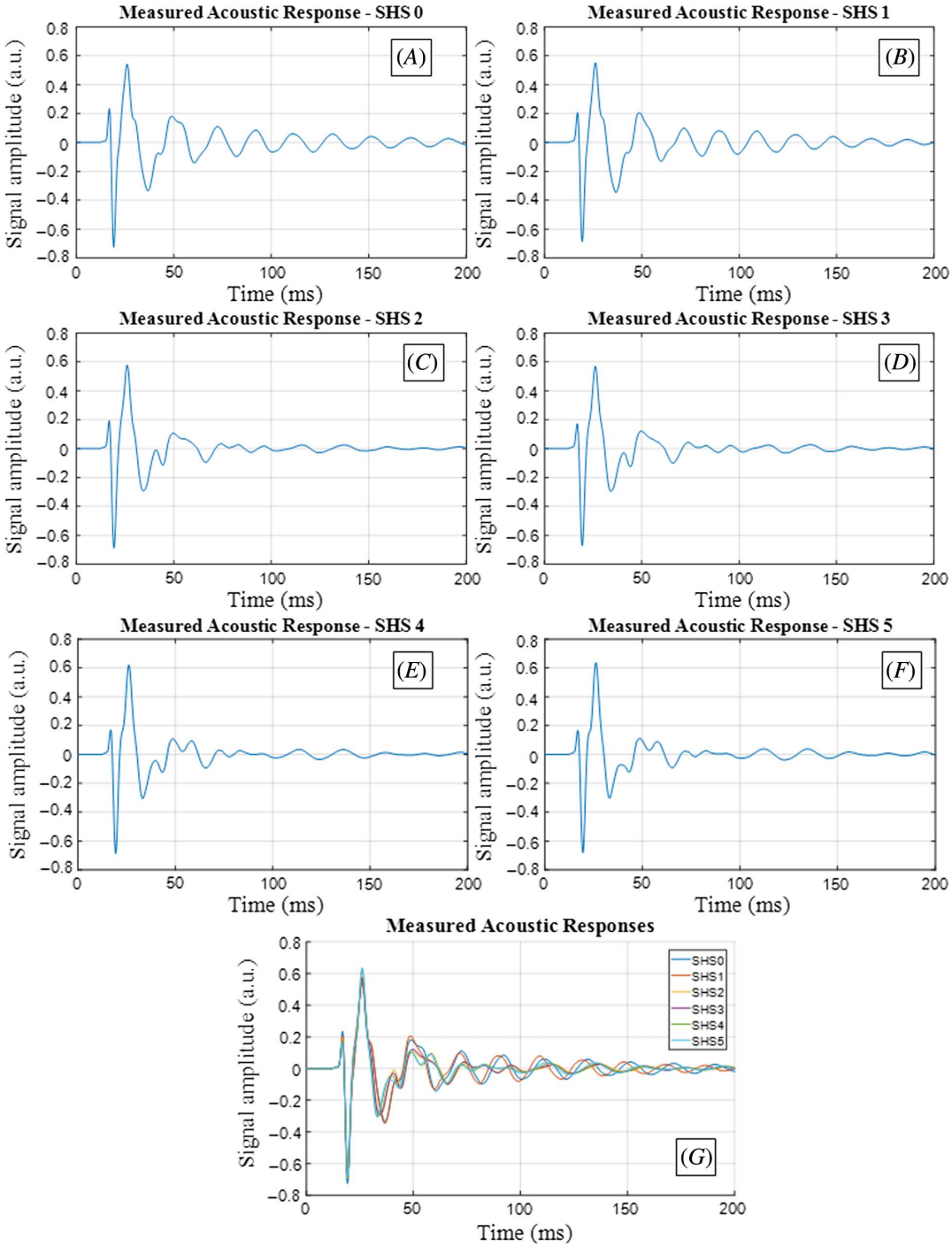

In the time-frequency domain, the Scalograms[40] (see fig. 7) show the scaled percentage of energy of the CWCs with different colors (or intensity variation of a single color, e.g., gray) with respect to time (or shift; x-axis) and scale variables (y-axis). The CWCs are calculated using the following expression[41]:

FIG. 6 Periodograms of the ARs of the road pavement to the LWD loads: structural health statuses 0 to 5 (*A*–*F*) and their comparison (*G*).

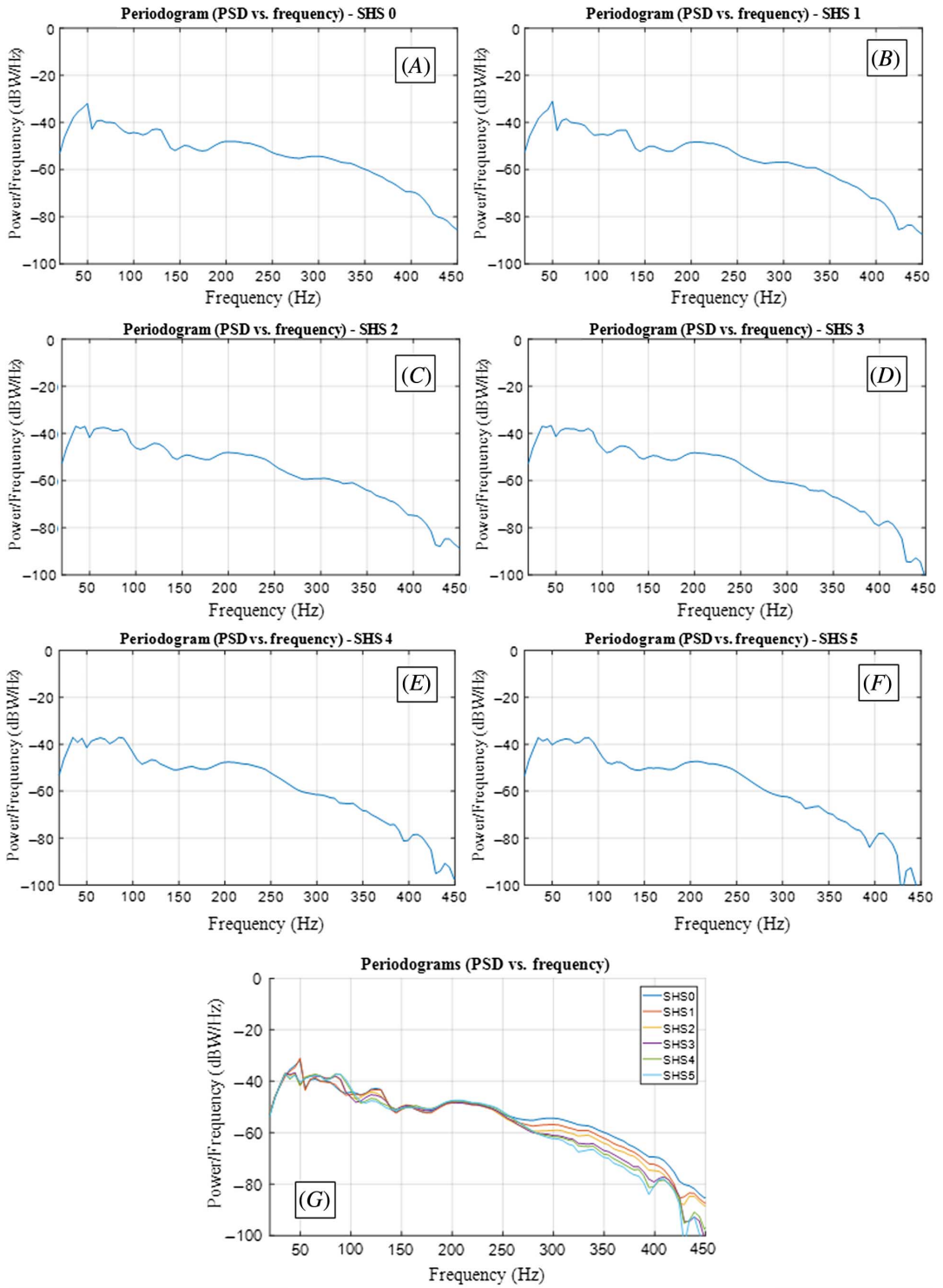

FIG. 7 Scalograms of the ARs of the road pavement to the LWD loads: structural health statuses 0 to 5 (*A–F*).

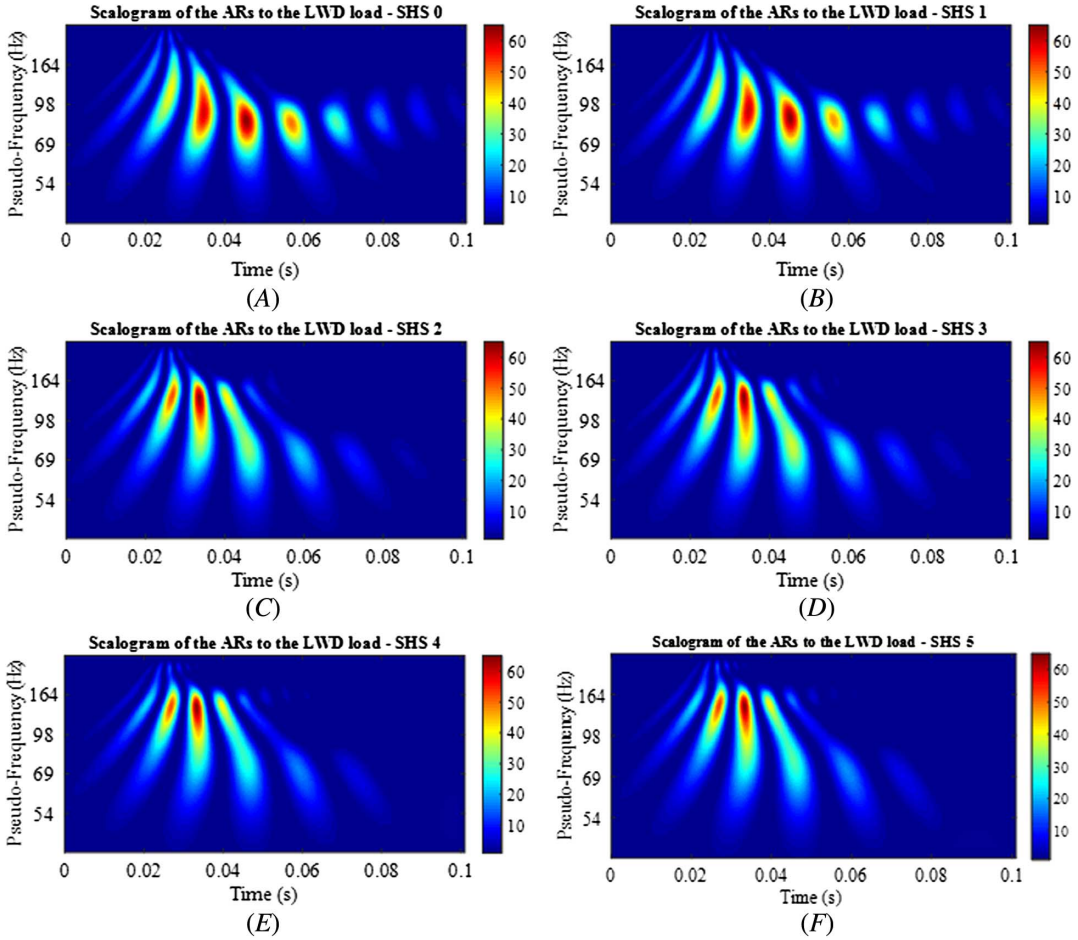

$$CWT(a,b) = \frac{1}{\sqrt{a}} \int x(t) \cdot \psi^* \left(\frac{t-b}{a} \right) dt, \tag{2}$$

where a is the scaling parameter (which allows contracting the mother wavelet ψ); b is the shifting parameter (which allows translating ψ along the x-axis [time]); $x(t)$ is the signal; t stands for time (seconds); and ψ^* is the complex conjugate of ψ. Furthermore, in order to have the frequency at the y-axis the following expression[42] was used, which allows derivation of the "pseudo-frequency":

$$F_a = \frac{F_c}{a} \cdot F_S, \tag{3}$$

where Fa is the pseudo-frequency (Hz) corresponding to the scale factor a (dimensionless); Fc is the central frequency of the mother wavelet ψ used (Hz); and F_S is the sampling frequency (Hz). In this study, the mother wavelet "morl" was used in the CWT.

Figure 5 shows (i) the average ARs (time domain) of the road pavement under test related to the 6 SHSs (form fig. 5*A* to 5*F*) that were taken into account in this study and (ii) the comparison among the ARs cited earlier (see fig. 5*G*). As is possible to see, the comparison shows how the presence of the drilled holes affects the ARs, which are more evident in the ARs' tails.

Figure 5 shows that the main phenomena last for less than 50 ms. Figure 6 illustrates the frequency content of ARs. Note that frequencies essentially range from 0 up to 450 Hz and the peak at 50 Hz tends to disappear when the SHS decays. Figure 7 depicts the Scalograms and highlights their effectiveness in providing information about not only frequency-related but also time-related differences.

As expected (cf. the statements in the introduction of the "Experimental Investigation" section), the presence of the artificial cracks mainly affected the spectral components of the AR of the road pavement. In particular, a decrease of the *PSD* in the frequency range 250–450 Hz can be noticed when the SHS of the road pavement goes from SHS0 to SHS5 (cf. fig. 6*G*). This decrease is associated with the presence of the holes in the road pavement.

FEM Modeling and Calibration

This section refers to FEM analysis (see figs. 8 and 9) and calibration (see figs. 10–20).

FIG. 8 Details extracted from the FEM model: (*A*) three-dimensional view of the modeled road pavement; (*B*) distance between LWD (source) and microphone (receiver); (*C*) detail of the LWD plate; (*D*) detail of the isolated microphone; (*E*) modeled road pavement with five lines of holes between the LWD and microphone; and (*F*) simulated impulse load.

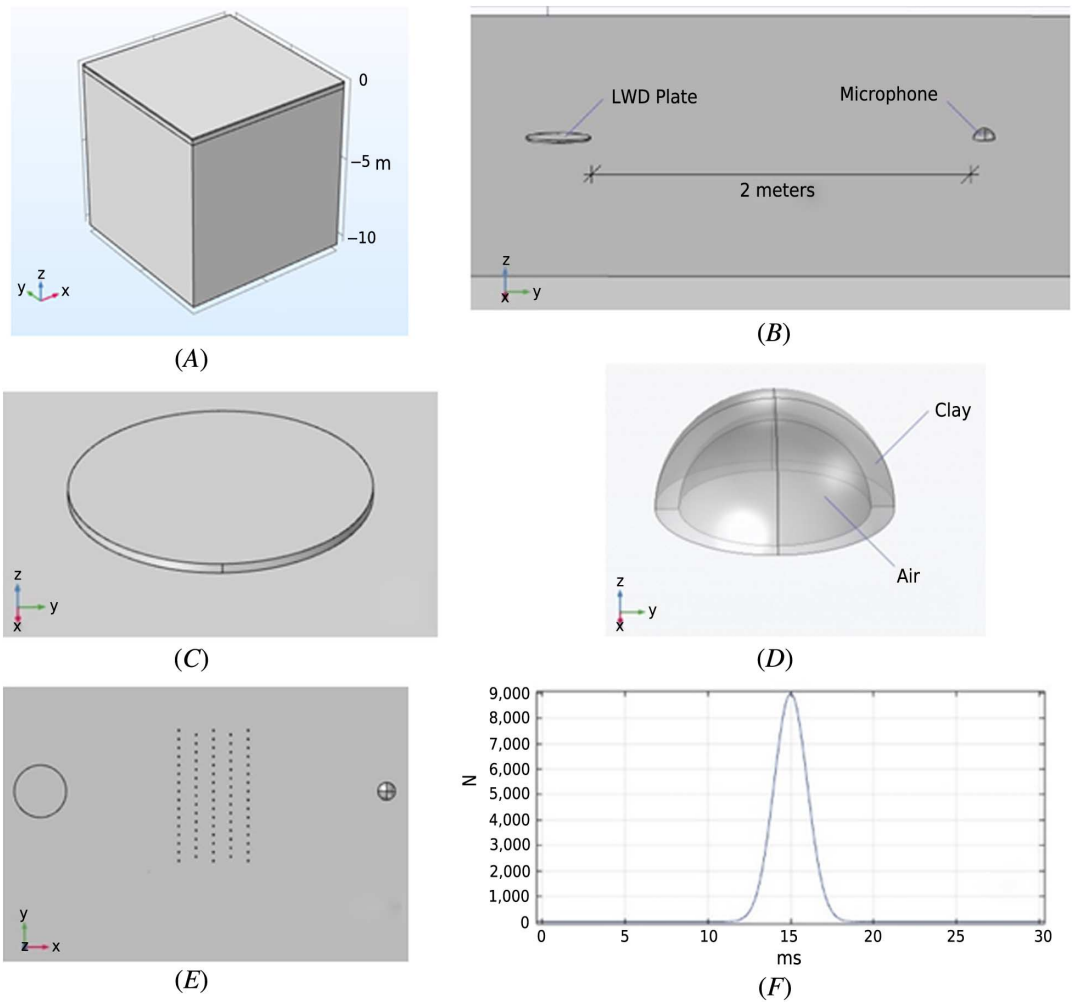

FIG. 9 Reference scenario: signals for SHS 0 to 5 (*A–F*), their comparison (*G*), and corresponding periodograms (*H*).

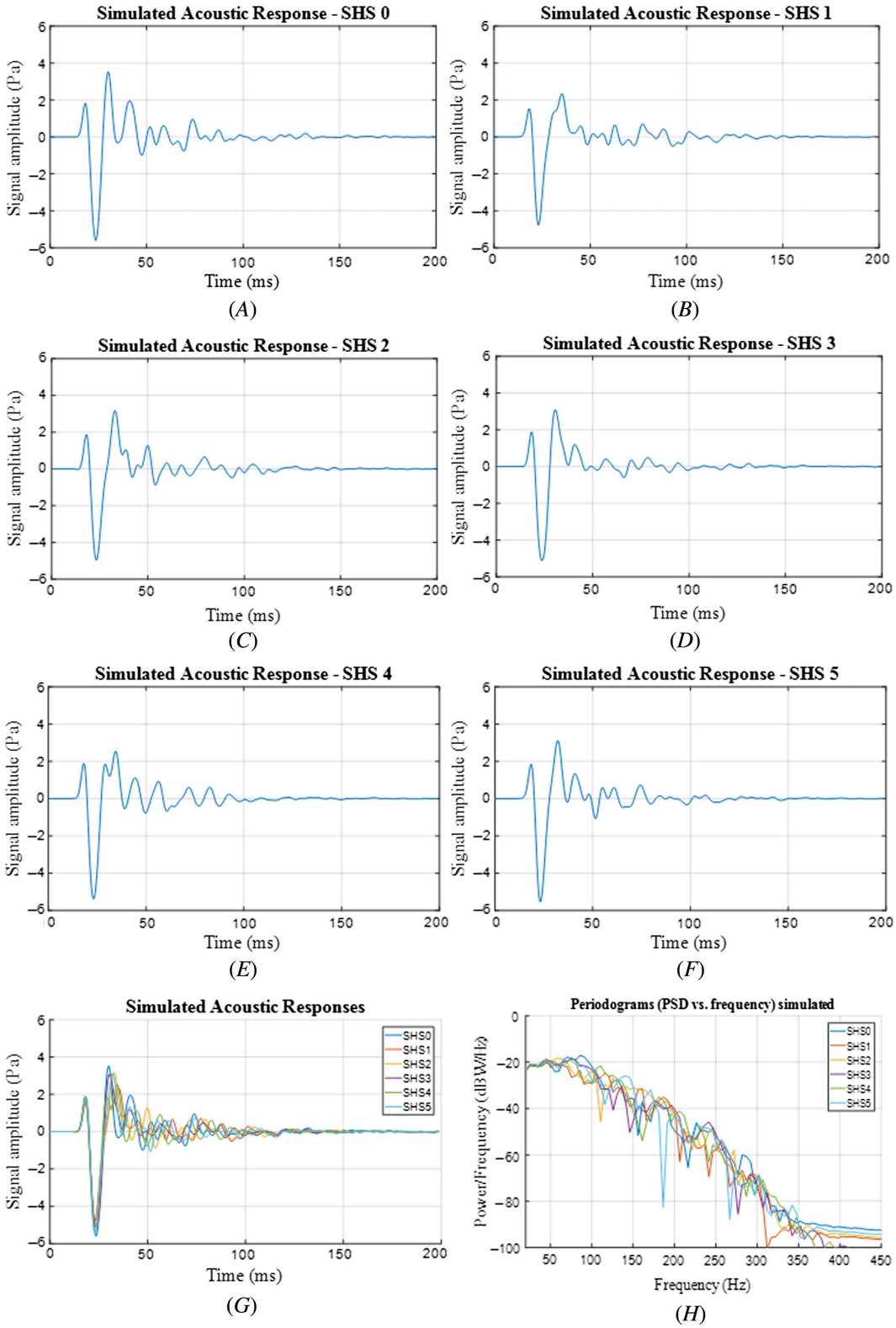

FIG. 10 Peaks of the (*A*) measured (Measured) and (*B*) simulated (FEM) signals used to calibrate the FEM model and (*C*) signal superposition.

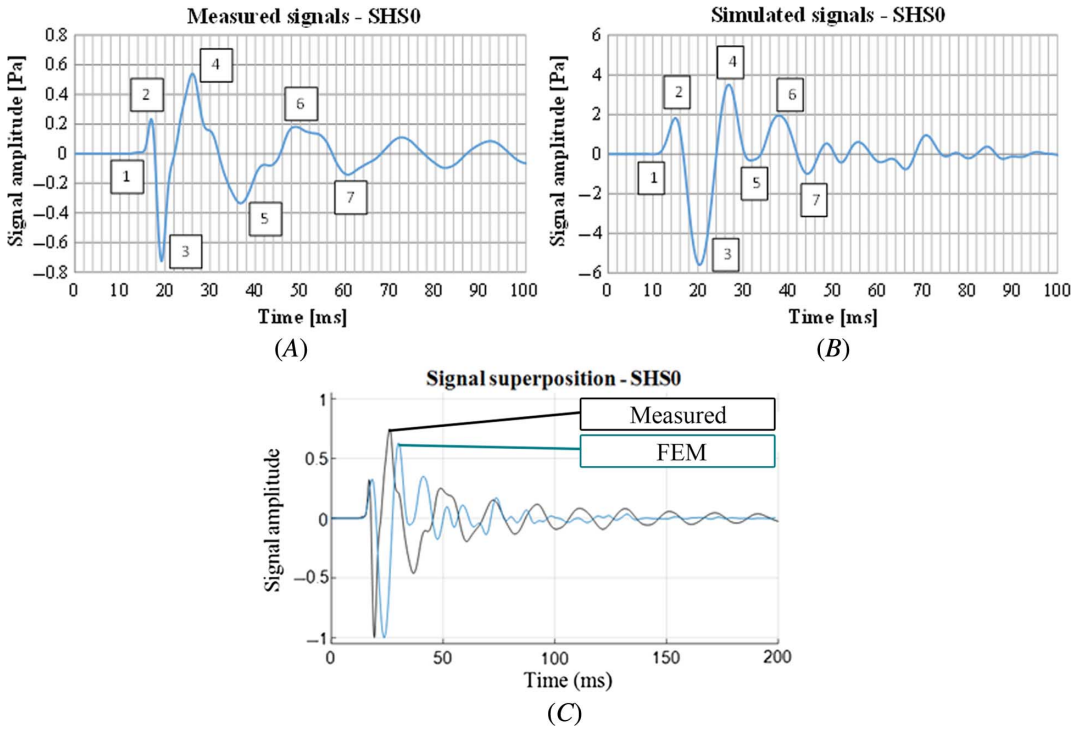

FIG. 11 FEM calibration: modulus effect on ordinate ratios y2/y3 to y7/y3 (*A*–*E*).

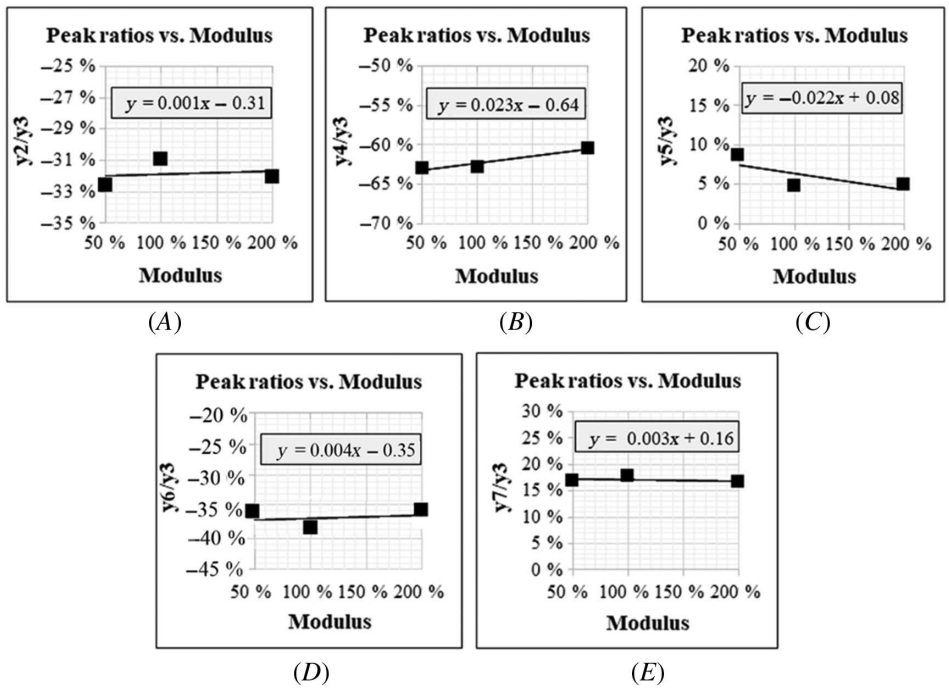

FIG. 12

FEM calibration: modulus effect on time lags x2-x1 to x7-x6 (*A–F*).

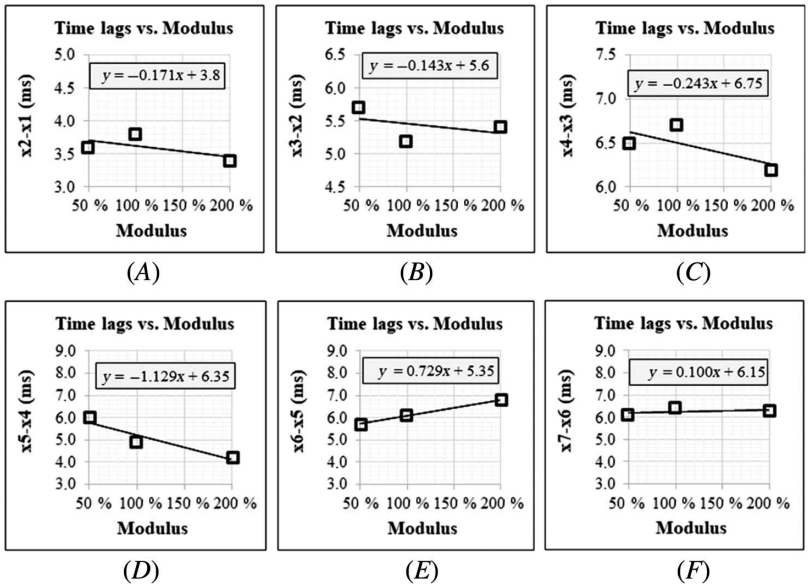

FIG. 13

FEM calibration: air temperature effect on ordinate ratios y2/y3 to y7/y3 (*A–E*).

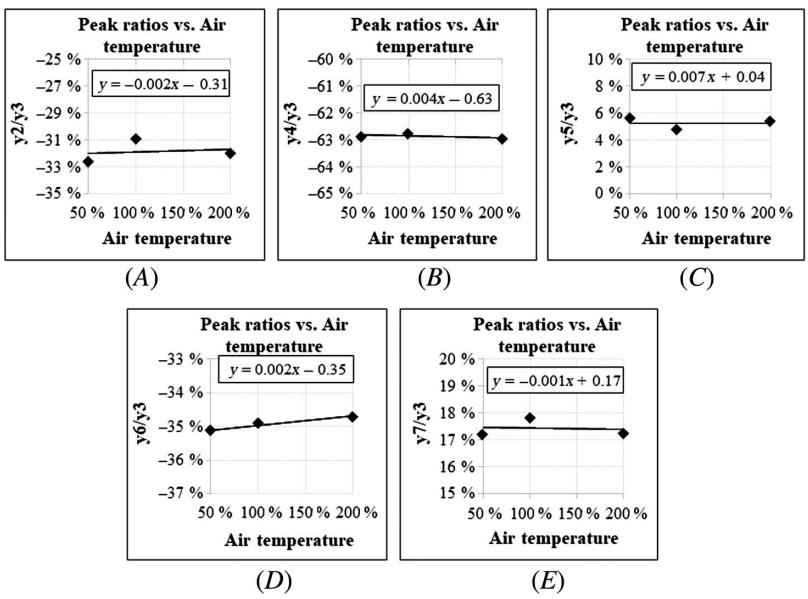

INTRODUCTION

In this study, the software COMSOL Multiphysics[43] was selected and used to model the responses of road pavements differently damaged to an impulsive load.

This software allows implementing a specific interface, i.e., the "Acoustic-Solid Interaction interface," which is designed to simulate the interactions between a solid body and sound waves. The output of a model built using this interface allows estimation of the deformation of the body due to a specific load, and the related

FIG. 14

FEM calibration: air temperature effect on time lags x2-x1 to x7-x6 (*A–F*).

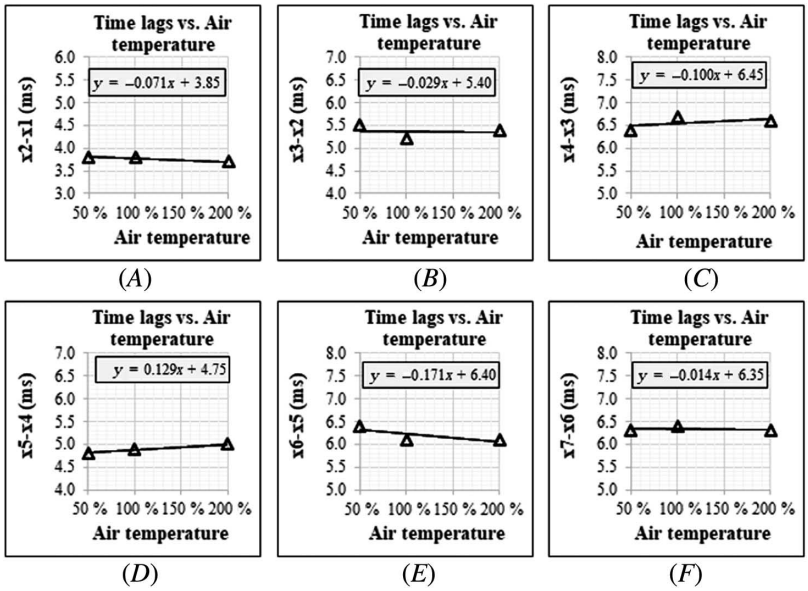

FIG. 15

FEM calibration: thickness effect on ordinate ratios y2/y3 to y7/y3 (*A–E*).

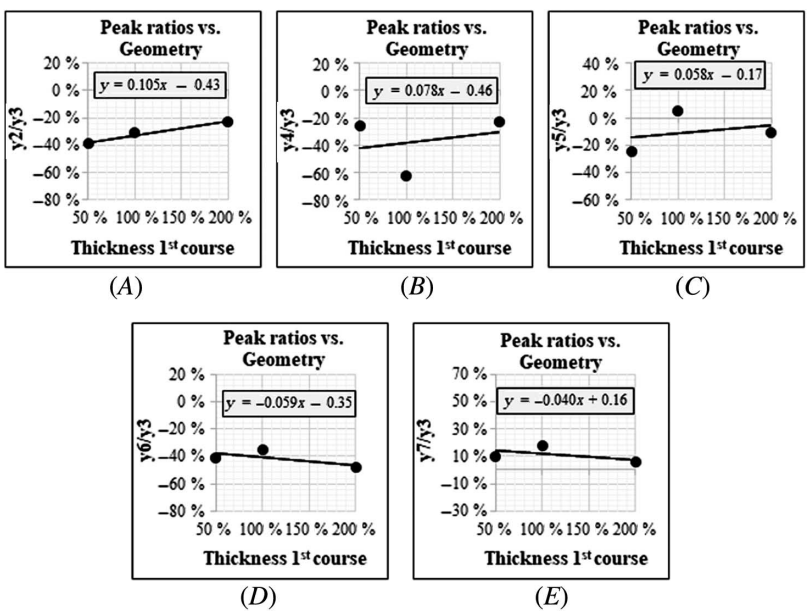

change of acoustic pressure around the faces of the body (i.e., across the fluid-solid boundary). In more detail, the structural acceleration acts on the fluid domain as a normal acceleration across the fluid-solid boundary.[43]

Furthermore, it allows studying these interactions in the time domain (transient signals) and frequency domain (frequency component and modal analysis).

FIG. 16

FEM calibration: thickness effect on time lags x2-x1 to x7-x6 (*A–F*).

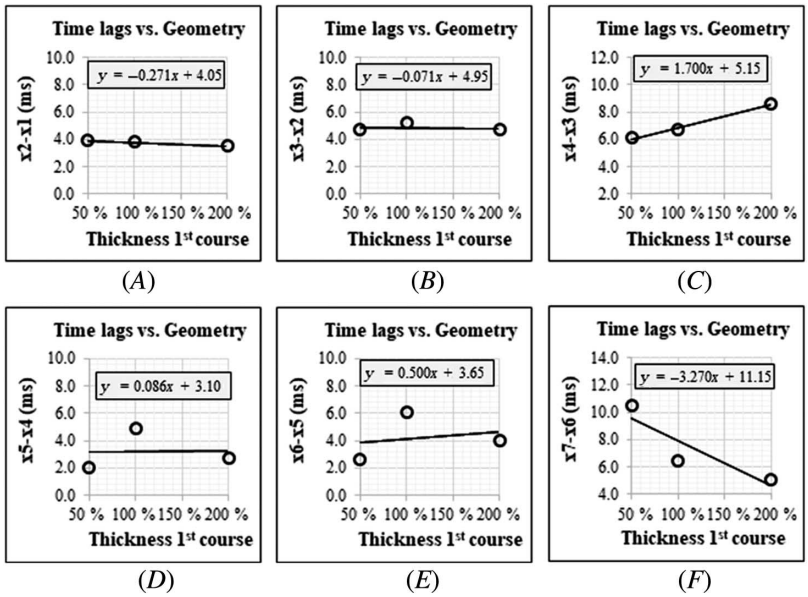

FIG. 17

FEM calibration: distance effect on ordinate ratios y2/y3 to y7/y3 (*A–E*).

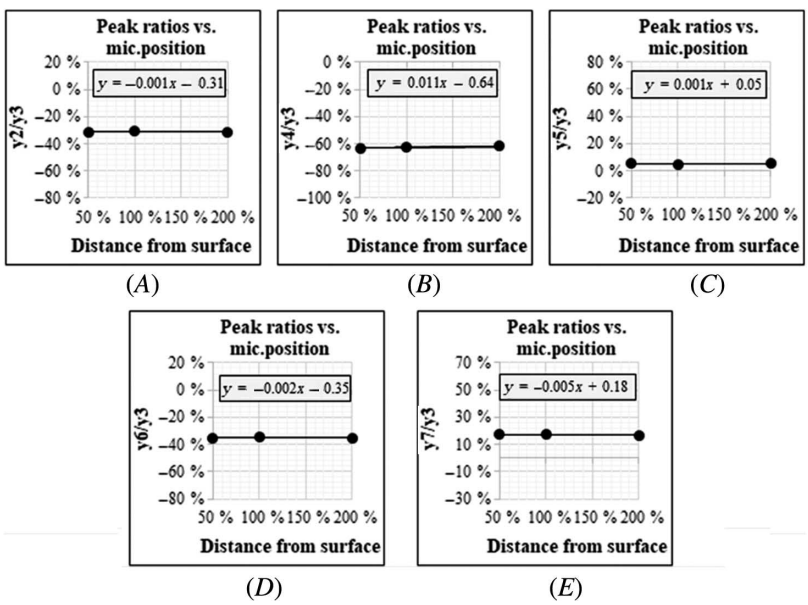

For the purposes of this study, among the possible studies included in the aforementioned interface, the Pressure Acoustics Transient study was selected.[43] In fact, it allows computation of the pressure variations due to the propagation of acoustic waves in fluids for given background conditions. By solving a scalar wave equation, it is possible to carry out time-dependent simulations, considering arbitrary time-dependent sources or fields. In addition, the same interface allows computing displacements, stresses, and strains by solving Navier's equations. [43]

FIG. 18

FEM calibration: distance effect on time lags x2-x1 to x7-x6 (*A–F*).

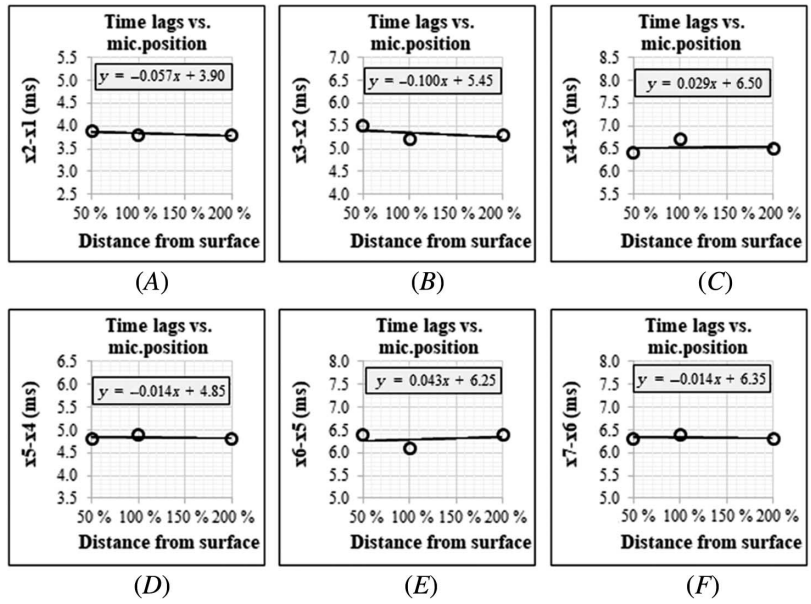

FIG. 19 FEM calibration: effect of unbound layer modulus on ordinate ratios y2/y3 to y7/y3 (*A–E*).

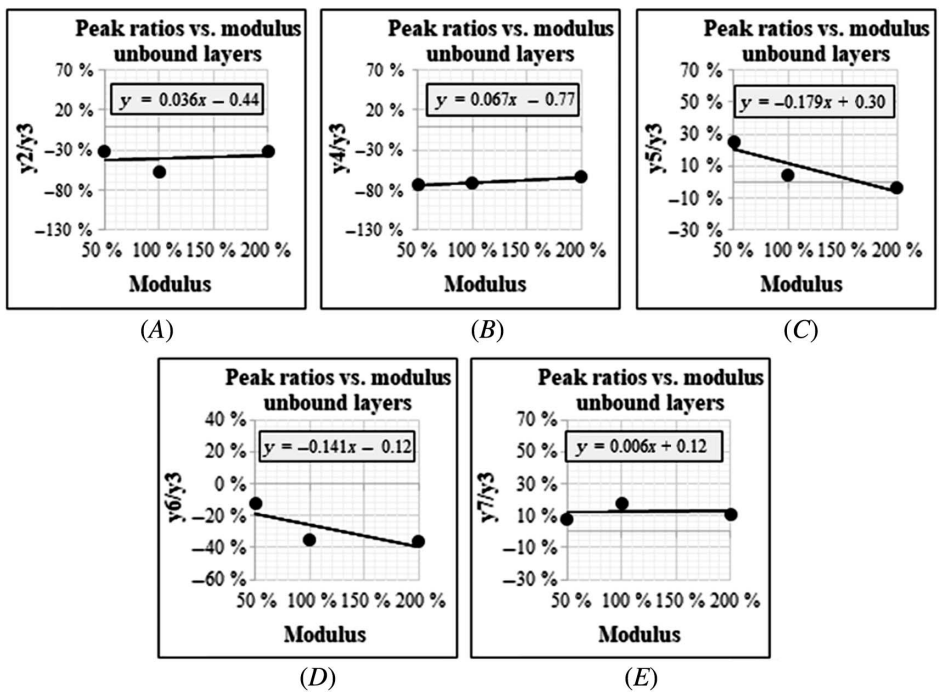

MAIN PARAMETERS OF FEM MODEL

The calibration of the model was carried out by adjusting the inputs and geometry of the FEM model in the pursuit of better simulating the experimental results.

FIG. 20 FEM calibration: effect of unbound layer modulus on time lags x2-x1 to x7-x6 (*A–F*).

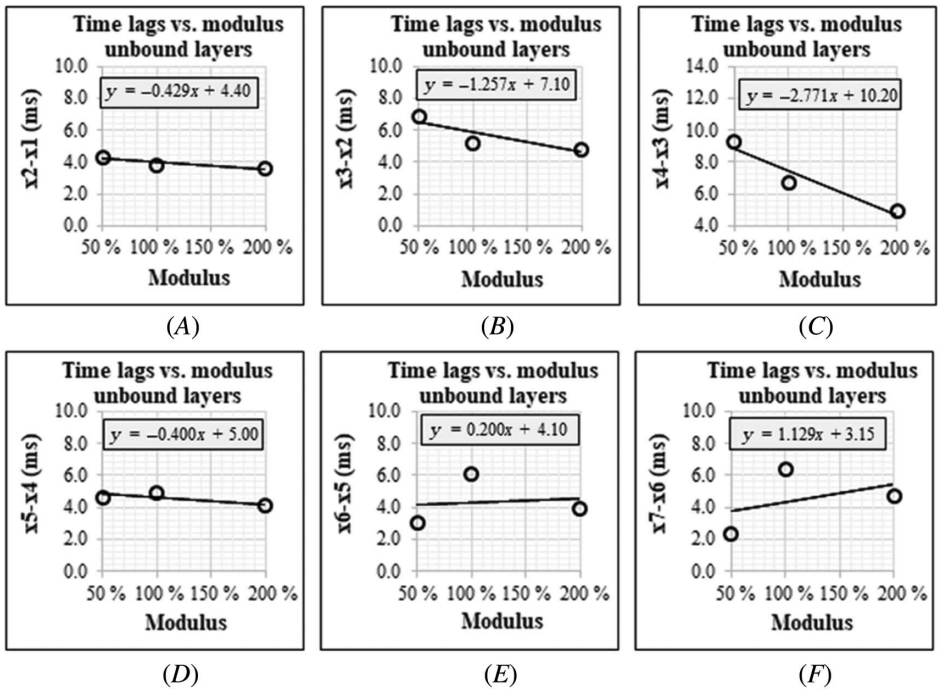

Overall, as inputs of the FEM model the following main parameters were considered: (i) magnitude, shape, and duration of the impulse load; (ii) dimensions of the objects involved (e.g., LWD base plate, road pavement layers, etc.); (iii) boundary conditions; and (iv) sampling frequency.

In more detail, the following main parameters were used in FEM analyses (reference scenario):

1. Geometry of the pavement and its boundary conditions (see fig. 8*A*). This includes the thickness of the layers (e.g., friction course and binder course: 0.1 m; subbase course: 0.3 m, cf. fig. 8*A*).
2. Position of sensors (microphone) and loads (LWD), cf. figures 4 and 8*B*.
3. Load-pavement interface (see fig. 8*C*). Steel was selected as material for the base plate of the LWD (Young's modulus = 200 GPa, density = 7,850 kg/m^3). The latter has the following dimensions: diameter = 30 cm and height = 1 cm.
4. The cap/dome over the microphone was modeled through a hemisphere (diameter = 10 cm, thickness = 1 cm), which is coated with white clay (Young's modulus = 50 MPa, Poisson's ratio = 0.3), and which contains air (temperature = 28°C). Finally, the boundary conditions "low reflection" were imposed to the hemisphere above.
5. Schematic of induced cracks in the pavement (see fig. 8*E*).
6. Load function over time (see fig. 8*F*). On average, the LWD used in the experimental investigation described in this study produced a force of 9 kN (because of a weight of 10 kg that falls from a height of 0.83 m and hits 5 "springs" [rubber buffers] with an average elastic constant of about 362 kN/m). The datasheet of the LWD indicates a typical range for the pulse time of 15÷30 ms (i.e., the duration of the LWD impulse load). In order to replicate this load in the FEM model, the following expression was used to build a pulse:

$$L = \frac{5 \cdot F}{\sigma\sqrt{2 \cdot \pi}} \cdot e^{-\frac{(t-\mu)^2}{2 \cdot \sigma^2}} \tag{4}$$

where L stands for load (N) as a function of t (time); σ corresponds to the standard deviation (that affects the width of the distribution, e.g., 2 ms); μ is the average time (that affects the position of the peak of the

pulse, e.g., 15 ms); t stands for time (ms); and F is a constant that refers to the impulse, force (e.g., 9 kN·ms). Note that according to Shivamanth et al.[44] and Ryden and Mooney,[45] the frequency spectrum of the LWD is mainly distributed in 0–300 Hz.

7. Main volumetric and mechanistic parameters: densities (e.g., 2,300 kg/m^3 for asphalt concretes), moduli (e.g., 1,000–2,000 MPa), and temperatures (e.g., 20°C–30°C).

FEM ARs FOR THE REFERENCE SCENARIO

Figure 9 shows the signals derived under the reference conditions (reference scenario, i.e., those described in the "Measured Signals in Three Domains of Analysis" section), prior to calibration analyses. Note that main part of ARs still refers to less than 50 ms, and the succession first wave positive, second wave negative, and third wave positive is still present.

AR CHARACTERISTICS USED TO CALIBRATE

The following main parameters were considered to compare experiments versus FEM results and carry out the calibration:

- Parameters in the time domain (i.e., ratios between peaks, distances along the x-axis of time, time lags);
- Parameters in the domain of frequencies (e.g., the slope of the linear regression of the Power Spectral Density in the Periodogram shown in figs. 6*G* and 9*H*);
- Parameters in the domain of time and frequencies (e.g., the maximum energy of the CWC, which is represented by the red parts of the Scalograms in fig. 7).

By referring to this preliminary study, figure 10 illustrates the main parameters used to compare FEM to experiments (e.g., peaks, domain of time; cf. fig. 10*A* and 10*B*). In other terms, in the domain of time, the goodness of fit of the FEM model was analyzed by comparing the aforementioned main peaks (FEM versus experiments) as a first step to the successive use of a cross-correlation method. The superposition between two corresponding signals is reported (see fig. 10*C*). It is possible to observe that in this case, the FEM signal is behind the signal obtained in experiments, while experimental time lags seem smaller than FEM ones.

Figure 10 shows that at a first stage, the simulated signal is quite different from the measured one. For this reason, the calibration procedure, described in the following section of the article, was carried out.

Results of Calibration

Figures 11–20 illustrate how the main parameters of the FEM model (e.g., asphalt concrete modulus) affect the indicators chosen to assess the goodness of the calibration (e.g., time lag between Points 4 and 5, x5-x4), for the cases in which the structural integrity was the highest (SHS0).

By referring to the analyses carried out in the domain of time, it is noted that the following main results were obtained.

Moduli, and particularly surface moduli, impact time lags and peak ratios (see figs. 11 and 12). To this end, it is noted that pavement temperature, which is a function of air temperature,[46,47] affects pavement moduli.[48,49] In figure 11, the peak ratios y4/y3, y2/y3, y5/y3, and y7/y3 are reported. It is possible to observe that, as expected, as far as the modulus of the friction course varies with respect to the reference scenario (in which the modulus is 100 %), there is not a clear trend toward higher and lower values.

Figure 12 illustrates how time lags (e.g., x6-x4, x5-x4) vary as a function of the modulus of the friction course. In this case, for x6-x5, the higher the modulus, the higher the time lag between the two peaks considered. Overall, the higher the modulus of asphalt concretes, the lower the time lags, except for the time lags x6-x5 and x7-x6.

Air temperature (see figs. 13 and 14) greatly affects time lags. Higher temperatures seem to correspond often to higher acoustic speeds and lower time lags. This implies that higher temperatures usually lead to lower time lags. The first derivative varies from +0.1 (x4-x3) to −0.17. Note that air temperature only has a tangible effect on the time lag between 3 and 4 (cf. fig. 14).

Figures 15 and 16 refer to the effect of asphalt layer thickness, whose assessment can be carried out through NDT or destructive testing (coring). Figure 15 illustrates how peak ratios vary when friction course thickness varies. Note that when x = 100 %, the majority of values tend to be the values measured in the experiments. For time lags, the thickness of the friction course only has a tangible effect on the time lag between 3 and 4 (cf. fig. 16).

Figures 17 and 18 deal with the distance of the microphone from the pavement surface. Note that the effect of the distance of the microphone from the pavement surface is quite negligible.

Figures 19 and 20 refer to how the modulus of unbound layers (beneath the asphaltic layers) affect FEM model outputs. The effect of the modulus of umbound layers on odinate ratios is quite negligible (except that for y6/y3, cf. fig. 19). The higher the modulus of unbound layers, the smaller time lags, usually (cf. fig. 20).

Figures 21 and 22 show the scatter diagrams that compare the measured data (experimental results) and simulated data (FEM model results) in terms of peak ratios (see fig. 21) and time lags (see fig. 22). The R-square coefficients of each distribution were calculated and range between 0.244 and 0.940. Based on this latter result, figure 23 reports the best result of the FEM model, i.e., the result corresponding to the maximum R square

FIG. 21

Comparison between simulated and measured data related to the peak ratios.

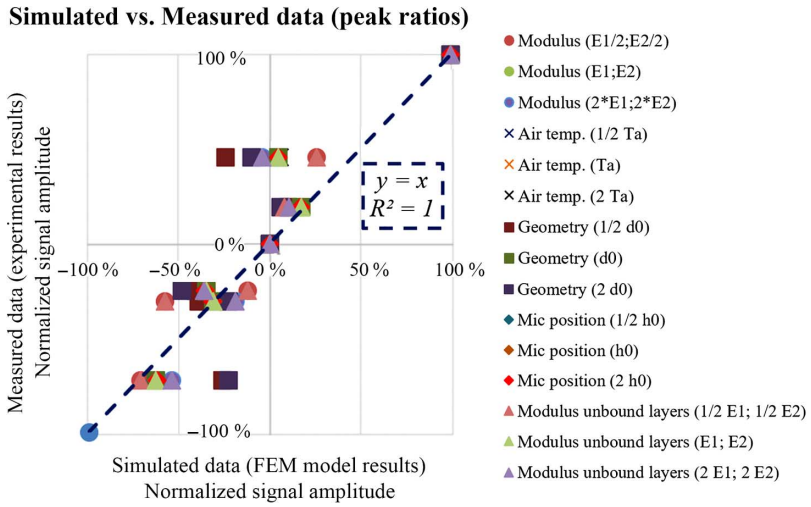

FIG. 22

Comparison between simulated and measured data related to the time lags.

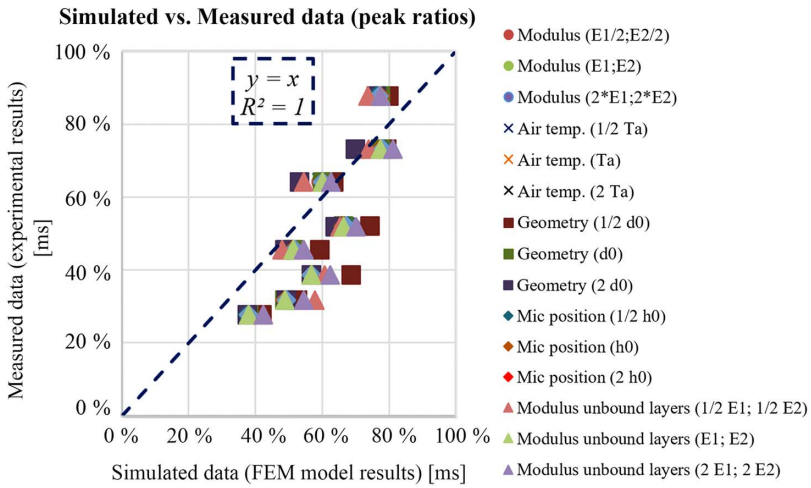

FIG. 23

Validation of the FEM model.

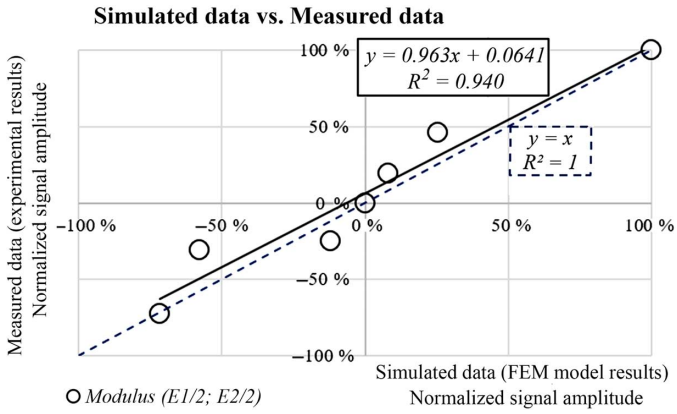

(i.e., 0.940). Importantly, this latter helps validate the FEM model. In fact, using the input parameters associated with the result shown in **figure 23** (i.e., halving the elastic moduli of the wearing course layer, E1, and binder layer, E2, according to the result of **fig. 11** and as reported in **fig. 23**), the simulated signal well approximates the measured signal. This is crucial in terms of validation of the FEM model proposed in this study.

Conclusions

An innovative, NDT-based system aiming at detecting concealed cracks in road pavements was set up and experiments were carried out. The study presented in this article aimed at modeling the involved phenomena through an FEM analysis and comparing data and simulations.

The software MATLAB was used to record the signals during the experiments, while the software Multiphysics® was used during the simulations.

Based on the results obtained, the following conclusions can be drawn:

- Air temperature and asphalt concrete moduli seem to play an outstanding role on the results of the FEM model presented in this article.
- Even if further studies are needed to better fix measurement chain and better carry out the FEM analyses, preliminary results show that the EXFEM is able to reproduce the measured signals and this model can be used to forecast the effects of different types of cracks on the propagation of vibrations into road pavements.
- Hence, the structural health conditions of a road pavement can be monitored using the measurement system to gather the acoustic signature of the pavement and the EXFEM to forecast the change of the acoustic signature over time because of the presence of the occurred cracks.

References

1. J. Moubray, "Proactive Maintenance (2): Predictive Tasks," in *Reliability-Centered Maintenance*, 2nd ed. (New York: Industrial Press, 1997), 144–167.
2. R. Fedele, F. G. Praticò, R. Carotenuto, and F. G. Della Corte, "Energy Savings in Transportation: Setting up an Innovative SHM Method," *Mathematical Modelling of Engineering Problems* 5, no. 4 (December 2018): 323–330. https://doi.org/10.18280/mmep.050408
3. C. Koch, K. Georgieva, V. Kasireddy, B. Akinci, and P. Fieguth, "A Review on Computer Vision Based Defect Detection and Condition Assessment of Concrete and Asphalt Civil Infrastructure," *Advanced Engineering Informatics* 29, no. 2 (April 2015): 196–210. https://doi.org/10.1016/j.aei.2015.01.008
4. J. Masino, J. Pinay, M. Reischl, and F. Gauterin, "Road Surface Prediction from Acoustical Measurements in the Tire Cavity Using Support Vector Machine," *Applied Acoustics* 125 (October 2017): 41–48. https://doi.org/10.1016/j.apacoust.2017.03.018

5. E. Schnebele, B. F. Tanyu, G. Cervone, and N. Waters, "Review of Remote Sensing Methodologies for Pavement Management and Assessment," *European Transport Research Review* 7, no. 7 (June 2015): 1–19. https://doi.org/10.1007/s12544-015-0156-6
6. Z. Tong, J. Gao, and H. Zhang, "Recognition, Location, Measurement, and 3D Reconstruction of Concealed Cracks Using Convolutional Neural Networks," *Construction and Building Materials* 146 (August 2017): 775–787. https://doi.org/10.1016/j.conbuildmat.2017.04.097
7. S. W. Katicha, G. Flintsch, J. Bryce, and B. Ferne, "Wavelet Denoising of TSD Deflection Slope Measurements for Improved Pavement Structural Evaluation," *Computer-Aided Civil and Infrastructure Engineering* 29, no. 6 (October 2014): 399–415. https://doi.org/10.1111/mice.12052
8. H. Hasni, A. H. Alavi, K. Chatti, and N. Lajnef, "A Self-Powered Surface Sensing Approach for Detection of Bottom-Up Cracking in Asphalt Concrete Pavements: Theoretical/Numerical Modeling," *Construction and Building Materials* 144 (July 2017): 728–746. https://doi.org/10.1016/j.conbuildmat.2017.03.197
9. C. Lenglet, J. Blanc, and S. Dubroca, "Smart Road That Warns Its Network Manager When It Begins Cracking," *Institution of Engineering and Technology Intelligent Transport Systems* 11, no. 3 (April 2017): 152–157. https://doi.org/10.1049/iet-its.2016.0044
10. B. F. Spencer Jr., H. Jo, K. A. Mechitov, J. Li, S.-H. Sim, R. E. Kim, S. Cho, et al., "Recent Advances in Wireless Smart Sensors for Multi-Scale Monitoring and Control of Civil Infrastructure," *Journal of Civil Structural Health Monitoring* 6, no. 1 (February 2016): 17–41. https://doi.org/10.1007/s13349-015-0111-1
11. Y. Wang, C. Ma, C. Sui, and P. Sung, "Natural Frequency Sensitivity Analysis of a Road Model Based on the Finite Element Method," *Journal of Engineering Science and Technology Review* 7, no. 2 (July 2014): 211–216. https://doi.org/10.25103/jestr.072.31
12. R. A. Tarefder, M. U. Ahmed, M. R. Islam, and M. T. Rahman, "Finite Element Model of Pavement Response under Load Considering Cross-Anisotropy in Unbound Layers," *Advances in Civil Engineering Materials* 3, no. 1 (January 2014): 57–75. https://doi.org/10.1520/ACEM20130102
13. P. Liu, D. Wang, and M. Oeser, "Application of Semi-Analytical Finite Element Method Coupled with Infinite Element for Analysis of Asphalt Pavement Structural Response," *Journal of Traffic and Transportation Engineering (English Edition)* 2, no. 1 (February 2015): 48–58. https://doi.org/10.1016/j.jtte.2015.01.005
14. P. Liu, D. Wang, J. Hu, and M. Oeser, "SAFEM – Software with Graphical User Interface for Fast and Accurate Finite Element Analysis of Asphalt Pavements," *Journal of Testing and Evaluation* 45, no. 4 (July 2017): 1301–1315. https://doi.org/10.1520/JTE20150456
15. L. Pedersen, "Viscoelastic Modelling of Road Deflections for Use with the Traffic Speed Deflectometer" (PhD thesis, Technical University of Denmark, 2013).
16. P. Cao, F. Jin, Z. Changjun, and D. Feng, "Investigation on Statistical Characteristics of Asphalt Concrete Dynamic Moduli with Random Aggregate Distribution Model," *Construction and Building Materials* 148, no. 1 (September 2017): 723–733. https://doi.org/10.1016/j.conbuildmat.2017.05.012
17. X. Tang and X. Yang, "Inverse Analysis of Pavement Structural Properties Based on Dynamic Finite Element Modeling and Genetic Algorithm," *International Journal of Transportation Science and Technology* 2, no. 1 (March 2013): 15–30. https://doi.org/10.1260/2046-0430.2.1.15
18. J. A. Hernandez and I. L. Al-Qadi, "Tire–Pavement Interaction Modelling: Hyperelastic Tire and Elastic Pavement," *Road Materials and Pavement Design* 18, no. 5 (July 2016): 1067–1083. https://doi.org/10.1080/14680629.2016.1206485
19. H. Moghimi and H. R. Ronagh, "Development of a Numerical Model for Bridge–Vehicle Interaction and Human Response to Traffic-Induced Vibration," *Engineering Structures* 30, no. 12 (December 2008): 3808–3819. https://doi.org/10.1016/j.engstruct.2008.06.015
20. M. A. Lak, G. Degrande, and G. Lombaert, "The Effect of Road Unevenness on the Dynamic Vehicle Response and Ground-Borne Vibrations Due to Road Traffic," *Soil Dynamics and Earthquake Engineering* 31, no. 10 (October 2011): 1357–1377. https://doi.org/10.1016/j.soildyn.2011.04.009
21. D. B. Casey, G. D. Airey, and J. R. Grenfell, "Relative Pavement Performance for Dual and Wide-Based Tire Assemblies Using a Finite Element Method," *Journal of Testing and Evaluation* 45, no. 6 (November 2017): 1896–1903. https://doi.org/10.1520/JTE20160589
22. T. Astrauskas and R. Grubliauskas, "Modelling of Ground Borne Vibration Induced by Road Transport," *Mokslas – Lietuvos Ateitis* 9, no. 4 (2017): 376–380. https://doi.org/10.3846/mla.2017.1060
23. D. H. Stamp and M. A. Mooney, "Influence of Lightweight Deflectometer Characteristics on Deflection Measurement," *Geotechnical Testing Journal* 36, no. 2 (March 2013): 216–226. https://doi.org/10.1520/GTJ20120034
24. Z. Dong, Y. Tan, L. Cao, and S. Li, "Rutting Mechanism Analysis of Heavy-Duty Asphalt Pavement Based on Pavement Survey, Finite Element Simulation, and Instrumentation," *Journal of Testing and Evaluation* 40, no. 7 (December 2012): 1228–1237. https://doi.org/10.1520/jte20120162
25. A. H. Alavi, H. Hasni, N. Lajnef, and K. Chatti, "Continuous Health Monitoring of Pavement Systems Using Smart Sensing Technology," *Construction and Building Materials* 114 (July 2016): 719–736. https://doi.org/10.1016/j.conbuildmat.2016.03.128
26. M. C. Guercio, Y. Mehta, and L. M. McCarthy, "Evaluation of Fatigue Cracking Performance of Asphalt Mixtures under Heavy Static and Dynamic Aircraft Loads," *Construction and Building Materials* 95 (October 2015): 813–819. https://doi.org/10.1016/j.conbuildmat.2015.07.025

27. S. Jingsong and H. Xiaoming, "The Damage Analysis of Asphalt Pavement under Repeated Loads," *Journal of Testing and Evaluation* 37, no. 5 (September 2009): 496–500. https://doi.org/10.1520/JTE003107
28. P. Liu, F. Otto, D. Wang, M. Oeser, and H. Balck, "Measurement and Evaluation on Deterioration of Asphalt Pavements by Geophones," *Measurement* 109 (October 2017): 223–232. https://doi.org/10.1016/j.measurement.2017.05.066
29. J. Gajewski and T. Sadowski, "Sensitivity Analysis of Crack Propagation in Pavement Bituminous Layered Structures Using a Hybrid System Integrating Artificial Neural Networks and Finite Element Method," *Computational Materials Science* 82 (February 2014): 114–117. https://doi.org/10.1016/j.commatsci.2013.09.025
30. K. Worden, C. R. Farrar, G. Manson, and G. Park, "The Fundamental Axioms of Structural Health Monitoring," *Proceedings of the Royal Society A* 463, no. 2082 (March 2007): 1639–1664. https://doi.org/10.1098/rspa.2007.1834
31. H. N. Li, L. Ren, Z.-G. Jia, T.-H. Yi, and D.-S. Li, "State-of-the-Art in Structural Health Monitoring of Large and Complex Civil Infrastructures," *Journal of Civil Structural Health Monitoring* 6, no. 1 (February 2016): 3–16. https://doi.org/10.1007/s13349-015-0108-9
32. E. Mesquita, P. Antunes, F. Coelho, P. André, A. Arêde, and H. Varum, "Global Overview on Advances in Structural Health Monitoring Platforms," *Journal of Civil Structural Health Monitoring* 6, no. 3 (July 2016): 461–475. https://doi.org/10.1007/s13349-016-0184-5
33. R. Fedele, F. Praticò, R. Carotenuto, and F. G. Della Corte, "Damage Detection into Road Pavements through Acoustic Signature Analysis: First Results" (paper presentation, 24th International Congress on Sound and Vibration, London, UK, July 23–27, 2017).
34. R. Fedele, F. G. Praticò, R. Carotenuto, and F. G. Della Corte, "Instrumented Infrastructures for Damage Detection and Management," in *Fifth IEEE International Conference on Models and Technologies for Intelligent Transportation Systems* (Piscataway, NJ: Institute of Electrical and Electronics Engineers, 2017), 526–531.
35. R. Fedele, M. Merenda, F. G. Praticò, R. Carotenuto, and F. G. Della Corte, "Energy Harvesting for IoT Road Monitoring Systems," *Instrumentation, Mesure, Métrologie* 17, no. 4 (December 2018): 605–623. https://doi.org/10.3166/i2m.17.605-623
36. R. Carotenuto, F. G. Della Corte, R. Fedele, M. Merenda, and F. G. Praticò. System and method for the structural monitoring of solid bodies to identify and monitor the growth of internal anomalies. Italy Patent 102017000133871, filed November 22, 2017.
37. W. A. Haupt, "Wave Propagation in the Ground and Isolation Measures" (paper presentation, Third International Conference on Recent Advances in Geotechnical Earthquake Engineering and Soil Dynamics, St. Louis, MO, April 2–7, 1995).
38. J. S. Bendat and A. G. Piersol, *Random Data Analysis and Measurement Procedures*, 4th ed. (Hoboken, NJ: John Wiley & Sons, 2010).
39. L. I. Slepyan and S. V. Sorokin, "Analysis of Structural-Acoustic Coupling Problems by a Two-Level Boundary Integral Method, Part 1: A General Formulation and Test Problems," *Journal of Sound and Vibration* 184, no. 2 (July 1995): 195–211. https://doi.org/10.1006/jsvi.1995.0312
40. M. M. Reda Taha, A. Noureldin, J. L. Lucero, and T. J. Baca, "Wavelet Transform for Structural Health Monitoring: A Compendium of Uses and Features," *Structural Health Monitoring* 5, no. 3 (September 2006): 267–295. https://doi.org/10.1177/1475921706067741
41. H. Kim and H. Melhem, "Damage Detection of Structures by Wavelet Analysis," *Engineering Structures* 26, no. 3 (February 2004): 347–362. https://doi.org/10.1016/j.engstruct.2003.10.008
42. A. Alhasan, D. J. White, and K. De Brabanterb, "Continuous Wavelet Analysis of Pavement Profiles," *Automation in Construction* 63 (March 2016): 134–143. https://doi.org/10.1016/j.autcon.2015.12.013
43. COMSOL Inc., "COMSOL Multiphysics," COMSOL Inc., 2018. https://web.archive.org/web/20190303044523/https://www.comsol.com/
44. A. Shivamanth, K. K. Pramod, P. S. Shama, K. D. Mayank, and K. D. Atul, "Study of the Light Weight Deflectometer and Reviews," *International Journal of Engineering Research and General Science* 3, no. 6 (November–December 2015): 42–46.
45. N. Ryden and M. A. Mooney, "Analysis of Surface Waves from the Light Weight Deflectometer," *Soil Dynamics and Earthquake Engineering* 29, no. 7 (July 2009): 1134–1142. https://doi.org/10.1016/j.soildyn.2009.01.002
46. M. J. C. Minhoto, J. C. Pais, P. A. A. Pereira, and L. G. Picado-Santos, "Predicting Asphalt Pavement Temperature with a Three-Dimensional Finite Element Method," *Transportation Research Record* 1919, no. 1 (January 2005): 96–110. https://doi.org/10.3141/1919-11
47. B. K. Diefenderfer, I. L. Al-Qadi, and S. D. Diefenderfer, "Model to Predict Pavement Temperature Profile: Development and Validation," *Journal of Transportation Engineering* 132, no. 2 (February 2006): 162–167. https://doi.org/10.1061/(asce)0733-947x(2006)132:2(162)
48. M. Halle, T. Rukavina, and J. Domitrovic, "Influence of Temperature on Asphalt Stiffness Modulus" (paper presentation, Fifth Eurasphalt & Eurobitume Congress, Istanbul, Turkey, June 13–15, 2012).
49. M. R. Taha, S. Hardwiyono, N. I. M. Yusoff, M. R. Hainin, J. Wu, and K. A. M. Nayan, "Study of the Effect of Temperature Changes on the Elastic Modulus of Flexible Pavement Layers," *Research Journal of Applied Sciences, Engineering and Technology* 5, no. 5 (February 2013): 1661–1667. https://doi.org/10.1080/0022027850170409